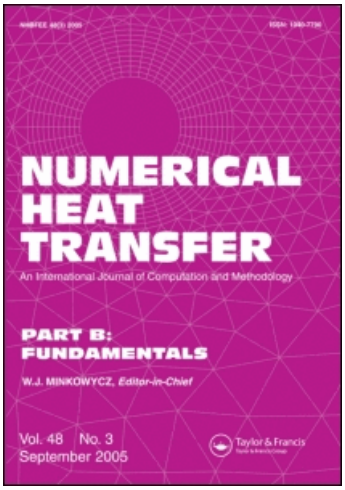

Numerical Heat Transfer, Part B: Fundamentals
Publication details, including instructions for authors and subscription information:
http://www.informaworld.com/smpp/title~content=t713723316

Enhanced Latent Heat Method to Incorporate Superheat Effects into Fixed-Grid Multiphysics Simulations

Seid Koric[a]; Brian G. Thomas[b]; Vaughan R. Voller[c]
[a] National Center for Supercomputing Applications, University of Illinois at Urbana-Champaign, Urbana, Illinois, USA [b] Department of Mechanical Science and Engineering, University of Illinois at Urbana-Champaign, Urbana, Illinois, USA [c] Department of Civil Engineering, University of Minnesota, Minneapolis, Minnesota, USA

Online publication date: 07 July 2010

To cite this Article Koric, Seid , Thomas, Brian G. and Voller, Vaughan R.(2010) 'Enhanced Latent Heat Method to Incorporate Superheat Effects into Fixed-Grid Multiphysics Simulations', Numerical Heat Transfer, Part B: Fundamentals, 57: 6, 396 — 413
To link to this Article: DOI: 10.1080/10407790.2010.496657
URL: http://dx.doi.org/10.1080/10407790.2010.496657

Numerical Heat Transfer, Part B, 57: 396–413, 2010

ISSN: 1040-7790 print/1521-0626 online
DOI: 10.1080/10407790.2010.496657

Taylor & Francis
Taylor & Francis Group

ENHANCED LATENT HEAT METHOD TO INCORPORATE SUPERHEAT EFFECTS INTO FIXED-GRID MULTIPHYSICS SIMULATIONS

Seid Koric[1], Brian G. Thomas[2], and Vaughan R. Voller[3]

[1]*National Center for Supercomputing Applications, University of Illinois at Urbana-Champaign, Urbana, Illinois, USA*

[2]*Department of Mechanical Science and Engineering, University of Illinois at Urbana-Champaign, Urbana, Illinois, USA*

[3]*Department of Civil Engineering, University of Minnesota, Minneapolis, Minnesota, USA*

An efficient new method has been developed to incorporate the effects of heat transfer in a liquid pool into models of heat conduction with solidification. The procedure has been added into the commercial package Abaqus [1] as a user-defined subroutine (UMATHT). Computational results of fluid flow and heat transfer in a liquid domain can be characterized by the heat flux crossing the boundary representing the solidification front, or liquidus temperature. This "superheat flux" can be incorporated into an uncoupled transient simulation of heat transfer phenomena in the mushy and solid regions by enhancing latent heat. The new method has been validated and compared to semianalytical solutions and two other numerical methods on simple test problems: two-dimensional, steady-state ledge formation in cryolite in aluminum extraction cells, and shell thinning in continuous casting of steel. Its real power, however, is for multiphysics simulations involving complex phenomena, such as solidification stress analysis with nonlinear constitutive equations. Including the superheat flux from a thermal-fluid flow simulation of the liquid pool into the latent heat provides a very efficient and robust method for incorporating the effects of fluid flow in the liquid pool into thermal-stress problems, especially for transient problems.

1. INTRODUCTION AND PREVIOUS WORK

As computer simulations of solidification processes mature, there is a growing need to include the effects of fluid flow into a thermomechanical analysis. The multiphysics approach of simulating all three phenomena (i.e., fluid flow, heat transfer, and stress) simultaneously is very computationally demanding and requires oversimplification of the individual phenomena [2, 3]. Some researchers attempt to

Received 23 March 2010; accepted 12 May 2010.

The authors would like to thank the Continuous Casting Consortium at the University of Illinois, Urbana-Champaign, the National Science Foundation for Grant DMI 05-28668, and the National Center for Supercomputing Applications (NSCA) for computational and software resources.

Address correspondence to Seid Koric, National Centre For Supercomputing Applications, University of Illinois at Urbana-Champaign, Mail Code 257, 1205 West Clark Street, Urbana, IL 61801, USA. E-mail: skoric@ncsa.illinois.edu

NOMENCLATURE

A	surface area
$[B]$	spatial derivative of [N]
c_p	specific heat
C	integration constants
erf	error function
H	enthalpy
H_f	latent heat
ΔH_f	latent heat increment
k	thermal conductivity
$[N]$	element shape functions
$\mathbf{n}$	surface unit normal vector
q	heat flux
t	time
Δt	time step
T	temperature
ΔT	temperature increment
$\mathbf{v}$	interface velocity
V	volume
$\mathbf{x}$	spatial coordinate
Δx	mesh spacing
α	thermal diffusivity
δ	interface position
ρ	density
ϕ	proportional constant
ω	relaxation factor

Subscripts

a	ambient (temperature)
bound	bound (integral)
eff	efficient (convection)
h	convection (surface)
i	NR iteration counter
in	internal (face)
init	initial (temperature)
k	spatial node counter
l	liquid
liq	liquid
melt	melting (temperature)
o	original
ref	reference (temperature)
s	solid
sh	super heat (heat coefficient)
sol	solid
super	super (heat)
surf	surface (temperature)

Superscripts

L	left
R	right
t	previous step time
$t+\Delta t$	current step time
T	transpose
$''$	flux superscript

decouple the thermal-fluid simulation from the stress analysis [4–8], but this neglects the important effects of shrinkage/deformation on heat transfer, such as that caused by pressure/gap formation between the casting and the mold [9–13]. Alternatively, the fluid flow simulation can be reasonably decoupled from the thermal-stress analysis if the liquid pool shape can be estimated *a priori*. Doing so is relatively easy for many processes involving a stable interface shape, such as ledge formation in cryolite electrolysis or the continuous casting of steel. Such simulations can readily output the "superheat flux" that delivers heat to the solidification front, such as that characterized by the liquidus temperature. This work investigates computational methods for solving heat conduction problems with solidification that can include the effect of the fluid flow by a "superheat flux."

Many different numerical methods have been developed to simulate heat conduction with phase change. Crank [14] and later Voller et al. [15, 16] have reviewed various techniques used for these problems. Front-tracking methods attempt to track the interface explicitly. For example, Juric and Tryggvason [17] use a fixed grid in space in which temperatures are calculated and a moving grid on the interface in which interface heat sources are computed. An immersed boundary method transfers information from the interface to the fixed grid. Segal et al. [18] used an adaptive moving grid that is introduced into the governing equations with an arbitrary Lagrangian Eulerian (ALE) approach.

Fixed-grid or latent heat methods [16, 19–24] offer general, simple, and robust alternatives to front-tracking methods. In these methods, phase change is accounted for by tracking the solid fraction or the change in enthalpy, H, across the interface, according to the latent heat released. These methods are easily implemented into existing heat transfer methods or codes and have been successfully applied to numerous phase-change problems [16, 19–24] and complex commercial solidification processes [10–13]. To predict microscale interfacial phenomena such as dendrite shape, "phase-field" methods characterize the solidification front as a field function which varies smoothly from 0 in the solid to 1 in the liquid, based on an assumed potential, such as Kobayashi [25] or Caginalp [26] as discussed elsewhere [27].

2. ENHANCED LATENT HEAT METHOD

2.1. Thermal Governing Equation and Its Finite Element Method Solution

In this new computational method, temperature in a fixed-grid domain including solid, liquid, and "mush" is found by solving the local form of the transient energy equation [28],

$$\rho\left[\frac{\partial H(T)}{\partial t}\right] = \nabla \cdot [k(T)\nabla T] \tag{1}$$

along with boundary conditions of prescribed temperature, prescribed heat flux, or the following surface convection condition:

$$(-k\nabla T)\cdot \mathbf{n} = h(T - T_a) \tag{2}$$

Using the finite-element method for spatial discretization and a fully implicit, two-level backward-difference algorithm for time integration [29], Eq. (1) becomes

$$\frac{1}{\Delta t}\int_v [N]^T \rho(H^{t+\Delta t} - H^t)\, dV + \int_v [B]^T k(T)[B]\, dV - \int_{A_h} [N]^T h(T - T_a)\, dA = 0 \tag{3}$$

where $[N]$ and $[B]$ contain the element shape functions and their spatial derivatives, respectively. Applying the Newton-Raphson iteration scheme gives the following linearized matrix equation:

$$\left[\frac{1}{\Delta t}\int_v [N]^T \rho\left(\frac{dH}{dT}\right)_i^{t+\Delta t} [N]\, dV + \int_v [B]^T k_i^{t+\Delta t}[B]\, dV - \int_{A_h} [N]^T h^1 [N]\, dA\right]\{\Delta T_{i+1}^{t+\Delta t}\}$$
$$= \int_{A_h} [N]^T h^1 (T_i^{t+\Delta t} - T_a)\, dA - \frac{1}{\Delta t}\int_v [N]^T \rho(H_i^{t+\Delta t} - H^t)\, dV - \int_v [B]^T k^t [B]\, dV \tag{4}$$

Equation (4) is solved for $\{\Delta T_i^{t+\Delta t}\}$ and then used to update the temperature solution, Eq. (5), until convergence is achieved at every point in the domain at time $t + \Delta t$:

$$\{T_{i+1}^{t+\Delta t}\} = \{T_i^{t+\Delta t}\} + \{\Delta T_{i+1}^{t+\Delta t}\} \tag{5}$$

2.2. Enhanced Latent Heat Method to Account for Superheat

To include the effect of superheat flux impinging on the solidification front, the model starts with the Stefan interface condition [30] that latent heat released due to interface displacement equals the net heat flux entering and leaving the interface:

$$k_s\left(\frac{\partial T}{\partial n}\right)_{\text{solid}} - k_l\left(\frac{\partial T}{\partial n}\right)_{\text{liquid}} = k_s\left(\frac{\partial T}{\partial n}\right)_{\text{solid}} - q''_{\text{super}} = \rho_s H_{f0}\frac{\partial \delta}{\partial t} \tag{6}$$

Where $\delta(t)$ is the time-dependant interface position (shell thickness), n is the direction normal to the solidification front, H_{f0} is the original latent heat of fusion, and heat flux delivered from liquid pool is called "superheat flux," q''_{super}.

Adding extra latent heat of fusion in the mushy zone to account for superheat flux coming from the liquid pool, Eq. (6) can be rewritten as

$$k_s\left(\frac{\partial T}{\partial n}\right)_{\text{solid}} = \rho_s(H_{f0} + \Delta H_f)\frac{\partial \delta}{\partial t} \tag{7}$$

Comparing Eqs. (6) and (7), the additional latent heat can be related to the superheat flux:

$$\Delta H_f = \frac{q''_{\text{super}}}{\rho_s v} \tag{8}$$

where $v = d\delta/dt$ is the instantaneous interface velocity.

Several possible methods can be used to find v in Eq. (8). In a transient numerical simulation, v can be estimated from the instantaneous temperatures, time increment size, and spatial gradients of temperature at every material point near the solidification front:

$$v = \frac{\Delta T}{\Delta t(\partial T/\partial n)} \tag{9}$$

This method produces excessive and fluctuating latent heat values when temperature increments ΔT are driven to be very small by the global NR iterative solution procedures in Eqs. (4) and (5), particularly at early simulation times and when superheat fluxes are high. It was found empirically that the maximum latent heat enhancement should be 30 to 40 times the original value in order to avoid these convergence problems and still provide an acceptable solution.

An alternative method is to estimate v based on analytical solutions for 1-D solidification. The simplest approach is a "quasi-stationary solution" [31], which replaces heat conduction Eq. (1) by the steady-state equation while allowing the phase-change front to advance in time. Quasi-stationary solutions have been derived for solidification of a semi-infinite plate on a chilled surface with an imposed temperature, heat flux, or convection boundary condition but are known to overestimate the interface location [31]. Instead, a new solution is derived here based on the

classical 1-D solid-control solidification solution [30] with the addition of superheat. The error-function solution in the semi-infinite solid [30, 31] is given by Eq. (10):

$$T(x,t) = C_1 + C_2 \mathrm{erf}\left(\frac{x}{\sqrt{4\alpha_s t}}\right) \tag{10}$$

Imposing boundary conditions of $T = T_{\mathrm{surf}}$ at $x = 0$, $T = T_{\mathrm{liq}}$ at $x = \delta(t)$ gives C_1 and C_2 and the temperature in the solid is

$$\frac{T(x,t) - T_{\mathrm{surf}}}{T_{\mathrm{liq}} - T_{\mathrm{surf}}} = \frac{\mathrm{erf}\left(x/2\sqrt{\alpha_s}\sqrt{t}\right)}{\mathrm{erf}(\phi)} \tag{11}$$

where ϕ is a proportionality constant for shell thickness growth, which increases with the square root of time:

$$\delta(t) = 2\phi\sqrt{\alpha_s}\sqrt{t} \tag{12}$$

The corresponding interface velocity is given by

$$v(t) = \frac{d\delta(t)}{dt} = \phi\sqrt{\alpha_s}\frac{1}{\sqrt{t}} \tag{13}$$

Using Eq. (11) to calculate flux coming from solid side of the interface, the Stefan condition in Eq. (6) becomes

$$\frac{k_s(T_{\mathrm{liq}} - T_{\mathrm{surf}})}{\sqrt{\pi}\mathrm{erf}(\phi)e^{\phi^2}} = \frac{1}{\sqrt{\alpha_s}\sqrt{t}} = \rho_s H_f \phi \frac{\sqrt{\alpha_s}}{\sqrt{t}} + q''_{\mathrm{super}} \tag{14}$$

which can be rearranged as

$$\frac{(T_{\mathrm{liq}} - T_{\mathrm{surf}})c_{ps}}{\sqrt{\pi}\left[H_f + \left(q''_{\mathrm{super}}/\rho\sqrt{\alpha_s}\phi\frac{1}{\sqrt{t}}\right)\right]} = \phi e^{\phi^2}\mathrm{erf}(\phi) \tag{15}$$

The above equation is solved for ϕ using the bisection rule [32]. Note that

$$\Delta H_f = \frac{q''_{\mathrm{super}}}{\rho v} = \frac{q''_{\mathrm{super}}}{\rho\sqrt{\alpha_s}\phi\frac{1}{\sqrt{t}}} \tag{16}$$

Equation (15) is identical to the known solid-control 1-D solidification solution with no superheat [30], except that total latent heat is updated here to include the enhanced latent heat due to superheat flux. This solution gives a very accurate and smooth estimate of the interface for a constant or near-constant surface temperature. For a surface flux or convective boundary condition, some form of time averaging of surface temperature can be applied, which provides a better velocity estimate than that of a quasi stationary solution.

2.3. Numerical Implementation

Equations (4) and (5) are solved with the commercial finite-element thermal-stress package Abaqus 6.8 [1], by creating a user subroutine UMATHT to implement the enhanced latent heat method for superheat flux, as described in this section. This subroutine is called at every material point during every global NR iteration, Eq. (4), and defines at the end of each increment: (1) internal thermal energy (enthalpy), (2) gradient of enthalpy with respect to temperature, and (3) heat flux vector.

The enthalpy gradient term $(dH/dT)^{t+\Delta t}$ is greatly enlarged over the phase-change temperature interval (mushy zone) $T_{\text{sol}} < T^{t+\Delta t}$ in Eq. (17) owing to the evolution of latent heat H_f. Here, T_{sol} and T_{liq} are the solidus and liquidus temperatures, respectively, and $c_p(T)$ is temperature-dependent specific heat, which is equal to $(dH/dT)^{t+\Delta t}$ outside the mushy zone.

$$\left(\frac{dH}{dT}\right)^{t+\Delta t} = c_p(T) + \frac{H_f^{t+\Delta t}}{(T_{\text{liq}} - T_{\text{sol}})} \tag{17}$$

The enthalpy at the end of the increment is updated via Eq. (18):

$$H^{t+\Delta t} = H^t + \left(\frac{dH}{dT}\right)^{t+\Delta t} \Delta T \tag{18}$$

In addition to latent heat, the heat flux vector at the end of the increment is updated in UMATHT from Fourier's law [28]:

$$\boldsymbol{q}'' = -k\frac{\partial T}{\partial x} \tag{19}$$

where the spatial temperature gradients $\partial T/\partial x$ are passed in from the main Abaqus code. To summarize the calculations performed for each material point in the mushy zone calling UMATHT:

1. Transcendental equation (15) is solved for ϕ.
2. Interface velocity is estimated from Eq. (13).
3. Latent heat enhancement ΔH_f is calculated from Eq. (8) and added to original latent heat of fusion H_{f0}.
4. Updated latent heat of fusion is used in Eq. (17) to calculate the enthalpy gradient.
5. Enthalpy is updated in Eq. (18), and the heat flux vector is updated in Eq. (19).

3. MOVING-GRID APPROACH

A moving-grid approach is applied here as an alternative method to solve two-dimensional steady solidification problems to demonstrate and validate the new latent-heat method. It is based on the steady-state control-volume finite-element method [33] employing bilinear quadrilateral elements. An example problem with a rectangular domain is illustrated in Figure 1. For the moving-grid method, the

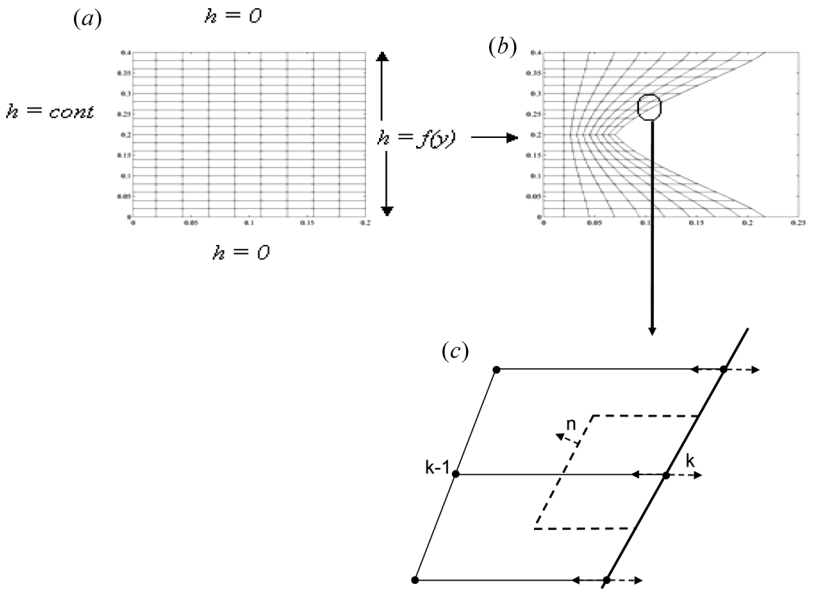

Figure 1. Schematic of moving-grid scheme.

domain is first covered with a mesh of rectangular bilinear elements. Here, heat transfer is governed by a steady-state heat conduction equation (20) with a constant conductivity. The upper and lower boundaries of the domain are insulated, while the left-hand boundary is subjected to a constant, nonzero heat transfer coefficient that and the right-hand boundary is subjected to a nonzero heat transfer coefficient that varies with vertical position y. Appropriate constants are set for the ambient temperatures on the left (T_a^L) and right (T_a^R).

The steady-state control-volume finite-element solution to this problem can be obtained for example node k in terms of nodal temperature values at the element vertices by applying finite-element approximations as follows:

$$\int_{\text{in}} K\nabla T \cdot \mathbf{n} dA = \int_{\text{bound}} h(y)(T_a^L - T)dA \approx h_k(T_a^L - T_k)\ell_{\text{bound}} \tag{20}$$

where, with reference to Figure 1, the integral "in" is over the internal faces of the control volume (see heavy dashed line), n represents the said faces, and the integral "bound" is over the control-volume faces coinciding with right-hand domain boundary (see heavy continuous line). The last term on the right side of Eq. (20) is obtained by applying a midpoint integration rule for the "bound" integral, where $h_k = h(y_k)$, ℓ_{bound} is the bound segment length, and a unit dimension into the page has been assumed.

For the solution of Eq. (20), the temperatures of nodes on the right-hand boundary vary with height (y). In a steady-state solution of a melting/solidification problem, however, these temperatures should take a constant value $T_k = T_{\text{melt}}$. To achieve this, the position of the nodes on the boundary must be adjusted through

the following iterative procedure. First, for the current guess of the domain geometry and grid, the steady-state control-volume finite-element problem is constructed and solved. Second, based on calculated right-hand boundary nodal values, the domain and mesh (nodal positions) are reset. A simple update scheme can force nodes to move, while maintaining a uniform spacing, along specified paths. Note that for this example problem, the paths are lines parallel to the x-axis.

Movement along a path is initiated by relocating the position of the node along a boundary. In the example problem, the movement along the x-axis is calculated from

$$\delta x_k = \omega \Delta x_k \frac{T_{\text{melt}} - T_k}{T_k - T_{k-1}} \tag{21}$$

where $0 < \omega \leq 1$ is a relaxation factor, and Δx_k is the current spacing along the kth path. After updating the domain and mesh, steps 1 and 2 are repeated until convergence, which is declared when, for all nodes k on the boundary, the temperature difference $T_{\text{melt}} - T_k$ is less then a prescribed tolerance. Note that more rapid convergence can be obtained by replacing the last term on the right side of Eq. (20) with $h_k = (T_a^L - T_{\text{melt}})\ell_{\text{bound}}$.

4. INTERNAL HEAT SOURCE METHOD

A simple explicit finite-difference method [34] is applied here as an alternative method to solve one-dimensional transient solidification problems, to further validate the new latent heat method. The superheat flux is applied as a heat source directly to the moving solidification front by searching at each time increment for the first interior node with a temperature below the liquidus temperature. The temperature at that node is adjusted to

$$T_k^{t+\Delta t} = T_k^{t+\Delta t} + \frac{\Delta t}{\rho c_p \, \Delta x} q''_{\text{super}}(t) \tag{22}$$

This method is implemented in a code, CON1D, [34] which has been coupled with a steady-state heat conduction model of a mold wall validated and applied successfully to simulate transient solidification in many commercial continuous casting processes. Further detail, including its extension to two dimensions in the code CON2D, can be found in [34, 35].

5. ONE-DIMENSIONAL TRANSIENT SOLIDIFICATION VERIFICATION PROBLEM

The method presented in Section 3 for modeling superheat by enhancing latent heat is tested here with a numerical analysis of a solidifying semi-infinite slab and an analytical solution for conduction with phase change [30], and with the conventional heat conduction method built into Abaqus [1]. The domain adopted for this problem is a thin slice through the shell shown in Figure 2. The domain and boundary conditions are shown in Figure 3. An instant quench of surface temperature to 1,200°C is imposed at the left boundary, with other boundaries insulated. A computationally challenging narrow mushy zone of 1°C between solidus and

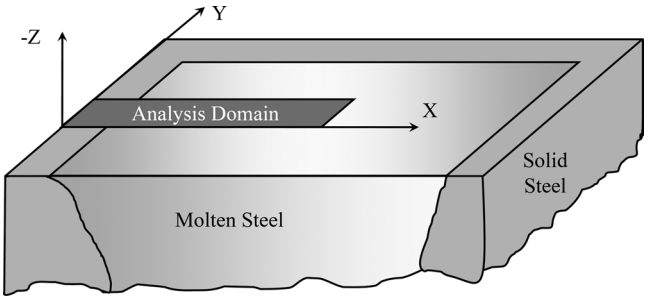

Figure 2. Solidifying slice.

liquidus is used to approximate the single melting temperature assumed in the analytical solution.

The material is a plane-carbon steel with properties listed in Table 1.

The superheat flux is best calculated with simultaneous modeling of fluid flow. For this simplified test problem, the superheat flux is driven by the temperature difference between T_{init} and T_{liq} assuming stagnant liquid. It is found by first solving the entire problem including the liquid pool starting from the initial temperature of T_{init} using the conventional solution method built into Abaqus. The heat flux shown in Figure 4 is extracted from that simulation as a function of time at the moving interface front (i.e., for the points that are at T_{liq} temperature). It represents the superheat flux entering the narrow mushy zone from the liquid pool. To illustrate the importance of superheat in this test problem, this case was rerun starting from the initial temperature of T_{liq}.

Next, the problem was rerun using the new enhanced latent heat method in Abaqus with UMATHT. Here, the initial temperature is T_{liq}, thus providing no superheat through the temperature difference between T_{init} and T_{liq}. Instead, the latent heat enhancement needed in Eq. (8) was calculated from the superheat flux in Figure 4.

Finally, an analytical solidification solution is also evaluated for comparison. For this example problem, the transcendental equation for ϕ takes a simplified form [30]:

$$\frac{c_p}{\sqrt{\pi}} e^{-\phi^2} \left[\frac{T_{\text{ref}} - T_{\text{surf}}}{\text{erf}(\phi)} - \frac{T_{\text{ref}} - T_{\text{init}}}{\text{erf}(\phi) - 1} \right] = H_f \phi \tag{23}$$

whose solution is found using Mathematica [36] and yielding $\phi = 0.43354$.

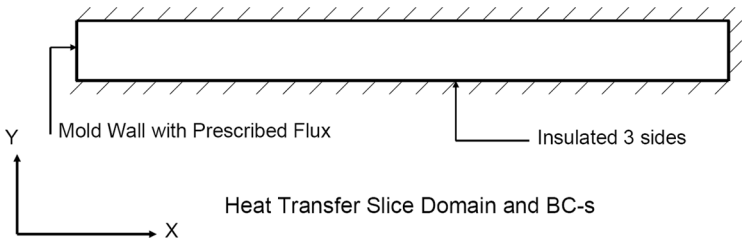

Figure 3. Solidifying slice domain and boundary conditions.

Table 1. Properties for 1-D verification problem

Symbol	Property	Value	Units
T_{liq}	Liquidus temperature	1,412.79	°C
T_{sol}	Solidus temperature	1,411.79	°C
T_{init}	Initial temperature	1,462.	°C
T_{ref}	Reference (melting) temperature	1,412.35	°C
T_{surf}	Surface temperature for analytical sol.	1,200	°C
k	Thermal conductivity of solid/liquid	35	W/m K
c_p	Specific heat of solid/liquid	620.	J/kg K
H_f	Latent heat of fusion	247,000	J/kg
α	Thermal diffusivity	7.18E-6	m^2/s
ρ	Density of solid liquid	7,860	kg/m^3
$L \times W$	Slice domain dimensions	30×0.1	mm
	Element size	0.1	mm

Temperature in the solid ($T < T_{ref}$) is given [30] by Eq. (24):

$$T(x,t) = T_{surf} + \frac{T_{ref} - T_{surf}}{\text{erf}(\phi)} \text{erf}\left(\frac{x}{2\sqrt{\alpha t}}\right) \tag{24}$$

Temperature in the liquid ($T > T_{ref}$) is given [30] by Eq. (25):

$$T(x,t) - T_{ref} = \frac{1}{\text{erf}(\phi) - 1}\left[T_{init}\text{erf}(\phi) - T_{ref} + (T_{ref} - T_{init})\text{erf}\left(\frac{x}{2\sqrt{\alpha t}}\right)\right] \tag{25}$$

For the case with no superheat, the transcendental equation for ϕ [30] simplifies to Eq. (26):

$$\phi e^{\phi^2}\text{erf}(\phi) = \frac{c_p(T_{ref} - T_{surf})}{\sqrt{\pi} H_f} \tag{26}$$

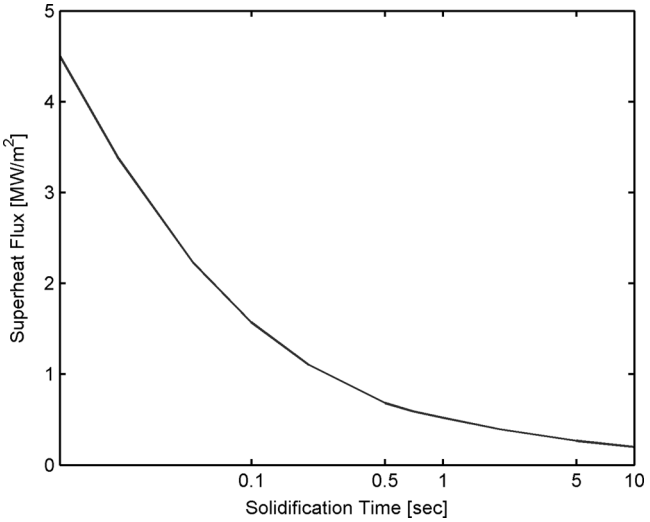

Figure 4. Superheat flux profile for 1-D validation problem.

yielding $\phi = 0.47786$; and temperature in the solid is given by Eq. (27) [30]:

$$\frac{T(x,t) - T_{\text{surf}}}{T_{\text{ref}} - T_{\text{surf}}} = \frac{\text{erf}(x/2\phi\sqrt{\alpha})}{\text{erf}(\phi)} \tag{27}$$

while in liquid it is equal to T_{liq}.

A comparison of shell thickness (defined by T_{ref}) between the standard method in Abaqus, the new enhanced latent heat method, and the analytical solution is shown in Figure 5. All three methods match closely for this test problem, both with and without superheat. Naturally, solidification is faster with no superheat. The new enhanced latent heat method is demonstrated to account accurately for superheat in this transient solidification problem.

Figure 6 shows the temperature distribution through the slice domain at 10 s for all five cases. The analytical temperature solution with superheat (solid line) is from Eqs. (24) and (25). The analytical solution with no superheat (dotted line) is from Eqs. (26) and (27). The circular symbols represent the standard Abaqus solution ($T_{\text{init}} = 1{,}462°\text{C}$). The diamond symbols represent the enhanced latent heat method for superheat with $T_{\text{init}} = T_{\text{liq}} = 1{,}412.79°\text{C}$. The square symbols represent the Abaqus solution with no superheat (i.e., with $T_{\text{init}} = T_{\text{liq}} = 1{,}462°\text{C}$, which is the same for both the standard and new methods.

Figure 6 shows that the three methods with superheat are almost identical in the solid, again indicating that the enhanced latent heat method can represent superheat effects accurately in the solid and mushy zones of interest. Within the liquid phase above the melting temperature, the enhanced latent heat method deviates as expected. This method starts with $T_{\text{init}} = T_{\text{liq}}$, and adds superheat to latent heat only in the solid and mushy zones (i.e., below $T_{\text{liq}} = T_{\text{init}}$). Temperature in the liquid is not

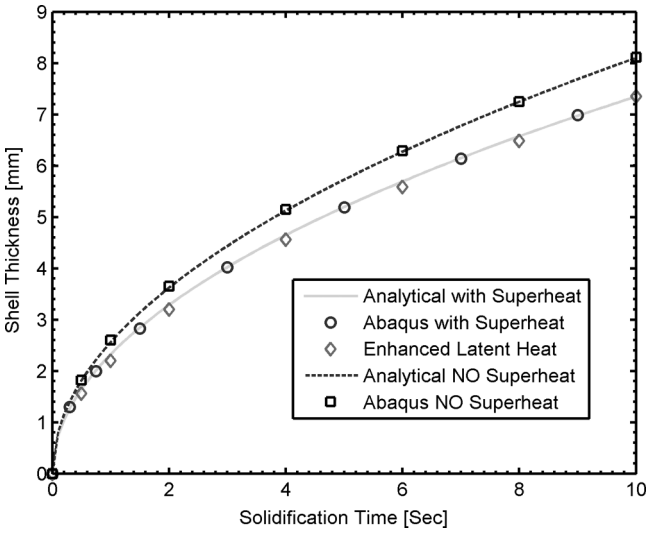

Figure 5. Shell thickness history comparison.

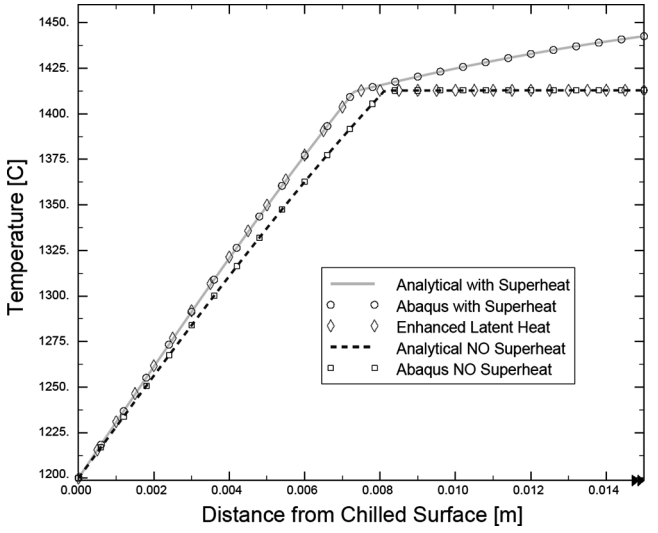

Figure 6. Comparison of temperature profiles at 2 s showing validation of enhanced latent heat method.

expected to be reasonable for any of these methods for realistic problems, and should be obtained from a prior analysis that includes fluid flow.

6. TWO-DIMENSIONAL STEADY MODEL OF SOLID CRYOLITE SHELL IN AN ALUMINUM REDUCTION CELL

The dynamic behavior of an aluminum reduction cell is a complex phenomenon affected by many physical processes in the pot. A schematic of one such process is shown in Figure 7, representing a two-dimensional thermal model of heat balance in an aluminum reduction cell. Since the problem in Figure 7 has the same boundary conditions as the example problem used to describe the moving-grid method in Section 3, the enhanced latent heat method is further validated here against the moving-grid method.

Superheat flux from the liquid pool in Eq. (28) is applied across the height of the solid shell/liquid cryolite interface (i.e., the vertical y direction), governed by a variable heat transfer coefficient h_{sh} in Eq. (29), which varies from 50 $\text{W/m}^2\,\text{K}$ (edge) to 2,000 $\text{W/m}^2\,\text{K}$ (center), and a constant liquid bath temperature of $T_{\text{init}} = 955.5^\circ\text{C}$. The resulting superheat flux varies between 275 and 11,000 W/m^2.

$$q''_{\text{super}} = h_{\text{sh}}(T_{\text{init}} - T_{\text{liq}}) \tag{28}$$

$$h_{\text{sh}} = 2,000. - 1,950.\sqrt{\frac{\text{Abs}(y - 0.2)}{0.2}} \tag{29}$$

The moving-grid code assumes a unique melting temperature, 950°C, which was modeled as an artificial mushy range of 1°C from $T_{\text{sol}} = 949^\circ\text{C}$ to $T_{\text{liq}} = 950^\circ\text{C}$ in Abaqus, making this problem even more numerically challenging for the enhanced latent heat method. The left edge is subject to convective cooling by ambient air with

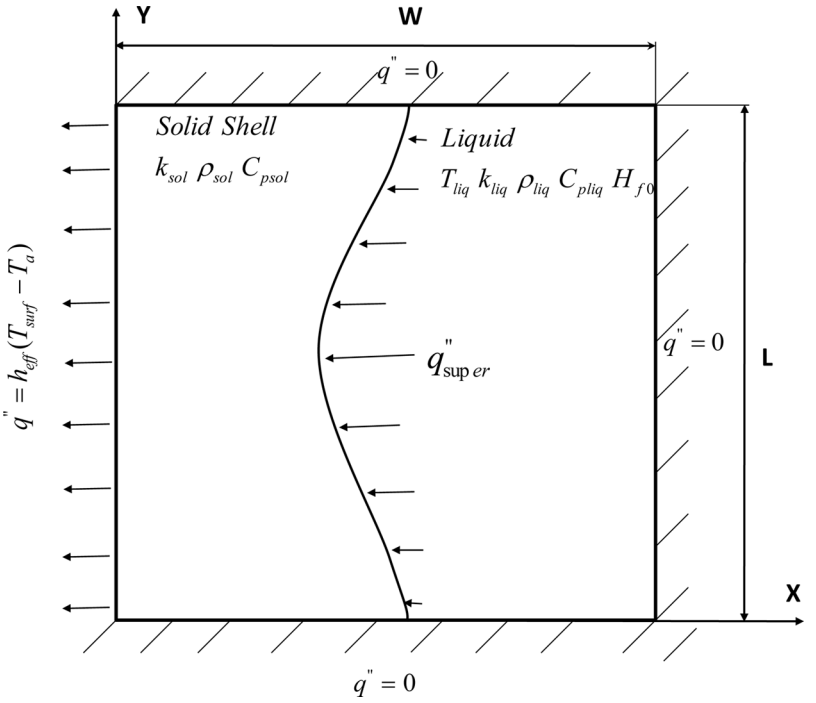

Figure 7. Aluminum reduction cell domain and boundary conditions.

$T_a = 30°C$ and $h_{eff} = 14.36\,W/m^2\,K$. The other three edges are thermally insulated. Other conditions are provided in Table 2.

Figure 8 shows the solidified ledge position calculated with the moving-grid and enhanced latent heat methods. The moving-grid method is very efficient

Table 2. Property and boundary conditions for 2-D test problem

Symbol	Property	Value	Units
T_a	Ambient temperature	30	°C
T_{liq}	Liquidus temperature	950	°C
T_{sol}	Solidus temperature	949	°C
T_{init}	Initial temperature	955.5	°C
T_{surf}	Average surface temperature	677.	°C
K_s	Thermal conductivity of solid	1.07	W/m K
K_l	Thermal conductivity of liquid	10.7	W/m K
C_{ps}	Specific heat of solid	1,800.	J/kg K
C_{pl}	Specific heat of liquid	1,800.	J/kg K
H_{f0}	Original latent heat of fusion	504,000	J/kg
ρ_s	Density of solid	2,850	kg/m^3
ρ_l	Density of liquid	2,850	kg/m^3
$W \times L$	Total domain dimensions	0.5×0.4	m
	Element size	10 and 2	mm
h_{eff}	Conv. heat transfer Coeff. shell/ambient	14.36	$W/m^2\,K$

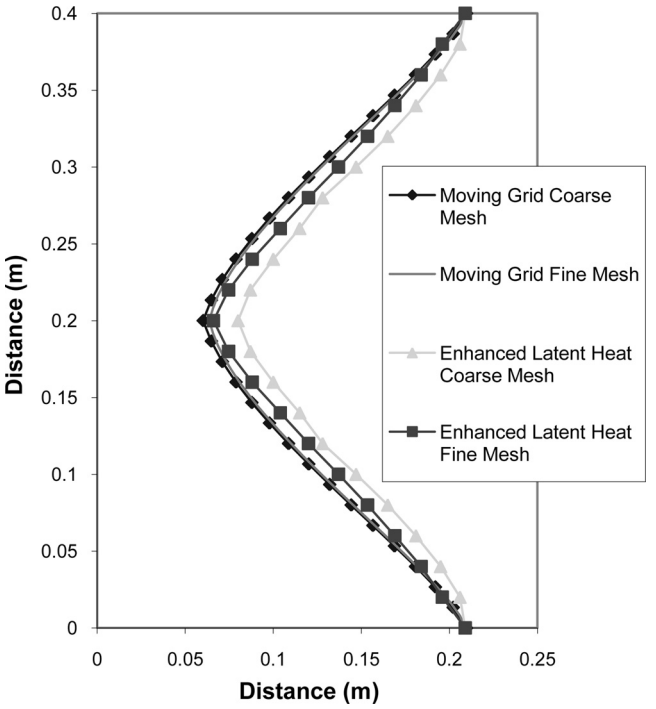

Figure 8. Steady-state ledge position comparison.

but is limited to a steady-state solution. The enhanced latent heat method must run a transient analysis for a long period (150,000 s) to approach the steady-state solution asymptotically, where the latent heat approaches infinity and the interface velocity approaches zero according to Eq. (8).

Mesh refinement studies were performed with both codes, bringing the best shell thickness results within 1 mm at the center, where the greatest errors are found. The results differed more with the coarse meshes. The edges show an almost perfect match in all cases. Both codes reveal a variation in shell thickness of 33% from edge to center. This is much less than the corresponding variation in superheat flux of 97.5%, and reflects the importance of two-dimensional conduction inside the solid ledge. The match between methods also shows that the very crude one-dimensional velocity estimate from Eqs. (13) and (15), based on an average surface temperature of 677°C, performs surprisingly well, even for this highly two-dimensional solidification problem. Moreover, the transient effects of ledge growth which are tracked by the new method as part of the solution are of great practical interest in their own right.

7. ONE-DIMENSIONAL TRANSIENT SOLIDIFICATION OF STEEL SHELL IN CONTINUOUS CASTING WITH NONLINEAR SUPERHEAT FLUX FROM FLUID JET IMPINGEMENT

In the final test problem, both the enhanced latent heat method and the internal heat source method [34] were applied to predict steel shell growth under realistic

Table 3. Properties for steel continuous casting simulation with superheat

Symbol	Property	Value	Units
T_{liq}	Liquidus temperature	1,477	°C
T_{sol}	Solidus temperature	1,502.2	°C
T_{init}	Initial temperature	1,502.24	°C
T_{ref}	Reference (melting) temperature	1,499.5	°C
K	Thermal conductivity of solid/liquid	26	W/m K
c_p	Specific heat of solid/liquid	680.	J/kg K
H_f	Orginal latent heat of fusion	243,000	J/kg
α	Thermal diffusivity	5.46E-6	m^2/s
ρ	Density of solid /liquid	7,000	kg/m^3

continuous casting conditions. The same solidifying slice domain from Figure 1 is used again in this analysis. All properties are listed in Table 3.

Previous work with a three-dimensional computational analysis of fluid flow in the continuous casting mold [37–39] yielded a nonlinear superheat flux profile along the narrow face, due to turbulent jet impingement. Figure 9 shows a superheat flux profile based on these analyses, which peaks at 400–600 mm below the meniscus. A realistic heat flux profile extracted from the mold wall [38] is also given in Figure 9, and is applied as a Neumann boundary condition at the chilled surface. The domain moves with the solidifying material at the casting speed of 25.4 mm/s. This Lagrangian approach has been validated in previous work [34].

Figure 10 shows shell thickness predictions with and without superheat along with plant measurements [40]. Both methods match and were able to capture the localized shell thinning effect caused by the peak in superheat flux where the jet impinges on the shell. The plant measurements are slightly displaced, owing to the transient nature of the breakout shell [41]. A comparison with the same case without superheat case reveals a profound difference in shell thickness. This further emphasizes the importance of accounting for the superheat effect in thermomechanical modeling of casting processes.

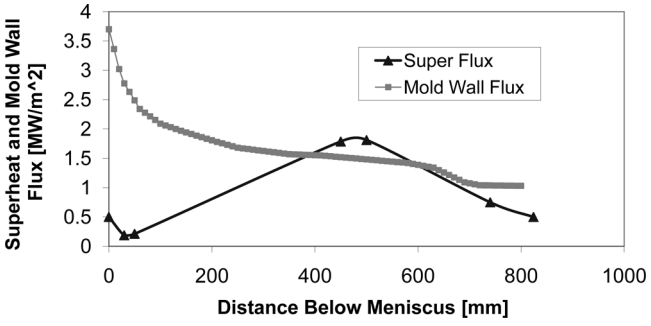

Figure 9. Realistic superheat and mold wall fluxes.

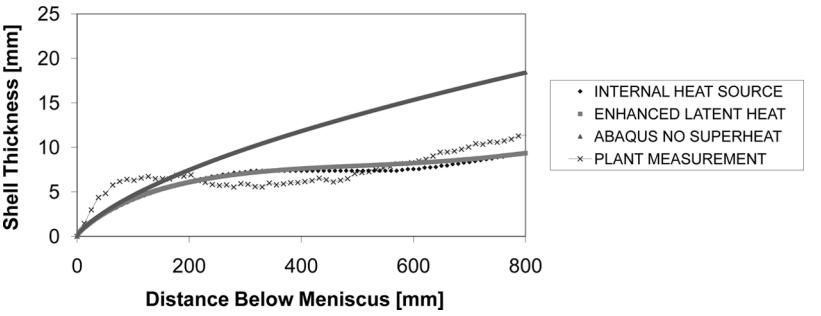

Figure 10. Shell thickness predictions and measurement.

8. CONCLUSION

A robust new algorithm to treat the effect of liquid superheat on moving solidification interfaces has been developed, coded into a UMATHT subroutine, and linked with the commercial finite-element code Abaqus. This ''enhanced latent heat'' method has been verified using both time-and spatially dependent superheat fluxes in one- and two-dimensional solidification problems, including a comparison with moving-grid and internal heat source methods from previous work.

The method developed in this work enables accurate uncoupling of complex heat transfer phenomena into separate simulations of the fluid flow region and the mushy-solid region. Spatially and temporally nonuniform superheat fluxes, produced by turbulent fluid flow and mixing in the liquid pool, are calculated from the results of computational fluid dynamics models [37–39]. The new latent heat method is used to link these results into coupled thermomechanical models of continuous casting using Abaqus [12, 13].

With this new method, future thermomechanical models of steel solidification can be more realistic, and also smaller, by avoiding the need for large liquid-filled volumes, which are prone to convergence problems. Such progress will, ultimately, lead to an efficient, accurate, and robust way to achieve multiphysics simulations of metal solidification on the continuum scale.

REFERENCES

1. *ABAQUS User Manuals v. 6.8*, Dassault Systems, Simulia Corp., 2008.
2. J. Lee, T. Yeo, Kyu H. OH, J. Yoon, and U. Yoon, Prediction of Cracks in Continuously Cast Steel Beam Blank through Fully Coupled Analysis of Fluid Flow, Heat Transfer, and Deformation Behavior of a Solidifying Shell, *Metal. Mater. Trans. A*, vol. 31A, pp. 225–237, 2000.
3. A. Teskeredzic, I. Demirdzic, and S. Muzaferija, Numerical Method for Heat Transfer, Fluid Flow, and Stress Analysis in Phase-Change Problems, *Numer. Heat Transfer B*, vol. 42, pp. 437–459, 2002.
4. A. Chatterjee, and V. Prasad, A Full 3-Dimensional Adaptive Finite Volume Scheme for Transport and Phase-Change Processes, Part I: Formulation and Validation, *Numer. Heat Transfer A*, vol. 37, pp. 801–821, 2000.

5. C. Del Borello and E. Lacoste, Numerical Simulation of the Liquid Flow into a Porous Medium with Phase Change: Application to Metal Composites Processing, *Numer. Heat Transfer A*, vol. 44, pp. 723–741, 2003.
6. J. Yang, Y. Du, R. Shi, and X. Cui, Fluid Flow and Solidification Simulation in Beam Blank Continuous Casting Process with 3D Coupled Model, *J. Iron Steel Res. Int.*, vol. 13, no. 4, pp. 17–21, 2006.
7. M. R. Shamsi and S. K. Ajmani, Three Dimensional Turbulent Fluid Flow and Heat Transfer Mathematical Model for the Analysis of a Continuous Slab Caster, *ISIJ Int.*, vol. 47, pp. 433–442, 2008.
8. M. Pokorny, C. Monroe, C. Beckermann, L. Bichler, and C. Ravindran, Prediction of Hot Tear Formation in Magnesium Alloy Permanent Mold Casting, *Int. J. Metalcasting*, vol. 2, no. 4, pp. 41–53, 2008.
9. K. Ho and R. D. Pehlke, Metal-Mold Interfacial Heat Transfer, *Metall. Trans. B*, vol. 16, pp. 585–594, 1985.
10. J. E. Kelly, K. P. Michalek, T. G. O'Connor, B. G. Thomas, and J. A. Dantzig, Initial Development of Thermal and Stress Fields in Continuously Cast Steel Billets, *Metall. Trans. A*, vol. 19A, pp. 2589–3602, 1988.
11. B. G. Thomas and M. Bellet, Modeling of Stress, Distortion, and Hot Tearing, in S. Viswanathan and E. DeGuire (eds.), *ASM Handbook vol. 15*, chap. 4G, ASM International, 2008.
12. S. Koric and B. G. Thomas, Efficient Thermo-Mechanical Model for Solidification Processes, *Int. J. Numer. Meth. Eng.*, vol. 66, pp. 1955–1989, 2006.
13. S. Koric and B. G. Thomas, *Thermo-Mechanical Model of Solidification Processes: Implementation in Abaqus and Application to Continuous Casting of Steel*, pp. 1–176, VDM-Verlag, Saarbrucken, Germany, 2009.
14. J. Crank, *Free and Moving Boundary Problems*, pp. 1–220, Oxford University Press, 1987.
15. V. R. Voller, An Overview of Numerical Methods for Solving Phase-Change Problems, *Adv. Numer. Heat Transfer*, vol. 1, no. 9, pp. 341–380, 1997.
16. R. Voller, C. R. Swaminathan, and B. G. Thomas, Fixed Grid Techniques for Phase Change Problems: A Review, *Int. J. Numer. Meth. Eng.*, vol. 30, pp. 875–898, 1990.
17. D. Juric and G. Tryggvason, A Front-Tracking Method for Dendritic Solidification, *J. Comput. Phys.*, vol. 123, pp. 127–148, 1996.
18. G. Segal, C. Vuik, and F. Vermolen, A Conserving Discretization for the Free Boundary in a Two-Dimensional Stefan Problem, *J. Comput. Phys.*, vol. 141, pp. 1–21, 1998.
19. V. R. Voller and M. Cross, Accurate Solutions of Moving Boundary Problems Using the Enthalpy Method, *Int. J. Heat Mass Transfer*, vol. 24, pp. 545–556, 1981.
20. B. G. Thomas, I. V. Samarasekera, and J. K. Brimacombe, Comparison of Numerical Modeling Techniques for Complex Two-Dimensional Transient Heat Conduction Problems, *Metal Mater. Trans. B*, vol. 15, pp. 307–318, 1984.
21. V. R. Voller, An Implicit Enthalpy Solution for Phase Change Problems: With Application to a Binary Alloy Solidification, *Appl. Math. Modell.*, vol. 11, pp. 110–116, 1987.
22. V. R. Voller, Enthalpy Method for Inverse Stefan Problem, *Numer. Heat Transfer B*, vol. 21, pp. 41–55, 1992.
23. C. K. Chun and S. O. Park, A Fixed-Grid Finite-Difference Method for Phase-Change Problems, *Numer. Heat Transfer B*, vol. 38, pp. 59–73, 2000.
24. B. Nedjar, An Enthalpy-Based Finite Element Method for Nonlinear Heat Problems Involving Phase Change, *Comput. Struct.*, vol. 80, pp. 9–21, 2002.
25. A. A. Wheeler, W. J. Boettinger, and G. B. McFadden, Phase Field Model for Isothermal Phase Transitions in Binary Alloys, *Phys. Rev. A*, vol. 45, pp. 7424–7439, 1992.
26. J. A. Mackenzie and M. L. Robertson, A Moving Mesh Method for the Solution of the One-Dimensional Phase Field Equations, *J. Comput. Phys.*, vol. 181, pp. 526–544, 2002.

27. M. Fabbri and V. R. Voller, The Phase Field Method in the Sharp-Interface Limit: A Comparison Between Model Potentials, *J. Comput. Phys.*, vol. 130, pp. 256–265, 1997.
28. R. W. Lewis, K. Morgan, H. R. Thomas, and K. N. Seetharamu, *The Finite Element Method in Heat Transfer Analysis*, pp. 1–290, Wiley, New York, 1996.
29. E. Feulvarch and J. Bergheau, An Implicit Fixed-Grid Method for the Finite-Element Analysis of Heat Transfer Involving Phase Change, *Numer. Heat Transfer B*, vol. 51, pp. 585–610, 2007.
30. J. A. Dantzig and C. L. Tucker III, *Modeling in Materials Processing*, pp. 282–321, Cambridge University Press, Cambridge, UK, 2001.
31. V. Alexiades and A. D. Solomon, *Mathematical Modeling of Melting and Freezing Processes*, pp. 125–161, Hemisphere Publishing Co., Washington, DC, 1993.
32. S. C. Chapra and R. P. Canale, *Numerical Methods for Engineers: With Software and Programming Applications* 4th ed., pp. 112–131, McGraw-Hill Higher Education, New York, 2002.
33. V. R. Voller, *Basic Control Volume Finite Element Methods for Fluids and Solids*, pp. 1–184, World Scientific, New Jersey, 2009.
34. Y. Meng and B. G. Thomas, Heat Transfer and Solidification Model of Continuous Slab Casting: CON1D, *Metal Mater. Trans. B*, vol. 34B, pp. 685–705, 2003.
35. C. Li and B. G. Thomas, Thermo-Mechanical Finite-Element Model of Shell Behavior in Continuous Casting of Steel, *Metal Mater. Trans. B.*, vol. 35B, pp. 1151–1171, 2005.
36. S. Wolfram, *The Mathematica Book,* 3rd ed., pp. 785–804, Cambride University Press, New York, 1998.
37. B. G. Thomas, R. O'Malley, T. Shi, T. Meng, D. Creech, and D. Stone, Validation of Fluid Flow and Solidification Simulation of a Continuous Thin Slab Caster, *Proc. Modeling of Casting, Welding and Advanced Solidification Processes*, vol. IX, pp. 769–776, 2000.
38. C. Pheiler, B. G. Thomas, A. Ludwig, and M. Wu, Solidification and Particle Entrapment during Continuous Casting of Steel, Proc. Steel Research Symposium 2007, Graz, Austria, 2007.
39. B. Zhao, B. G. Thomas, S. P. Vanka, and R. J. O'Malley, Transient Fluid Flow and Superheat Transport in Continuous Casting of Steel Slabs, *Metal Mater. Trans. B*, vol. 36(B), pp. 801–823, 2005.
40. Y. Meng and B. G. Thomas, Simulation of Microstructure and Behavior of Interfacial Mold Slag Layers in Continuous Casting of Steel, *Proc. ISIJ International 2006*, vol. 46, pp. 660–669, 2006.
41. B. G. Thomas, R. J. O'Malley, and D. T. Stone, Measurements of Temperature, Solidification, and Microstructure in a Continuous Cast Thin Slab, *Proc. Modeling of Casting, Welding, and Advanced Solidification Processes MCWASP VIII*, pp. 1185–1199, 1998.